Two-dimensional numerical analysis on the rock/bolt interaction considering shear and normal relative displacements

Two-dimensional numerical analysis on the rock-bolt interaction considering shear and normal relative displacements

Pierpaolo Oreste[1], Giovanni Spagnoli[2]*

[1] Department of Environment, Land and Infrastructure Engineering, Politecnico di Torino, Corso Duca Degli Abruzzi 24, 10129 Torino, Italy; *pierpaolo.oreste@polito.it*

[2] DMT GmbH & Co. KG, Am TÜV 1, 45307 Essen, Germany, *giovanni.spagnoli@dmt-group.com* ORCID: 0000-0002-1866-4345 (CORRESPONDING AUTHOR)

Abstract

Fully grouted passive bolts are widely used in underground or surface rock excavations and in particular in stabilizing potentially unstable blocks of rock due to sliding on natural discontinuities. Their operating mechanism is complex, but it is possible to consider two stabilizing forces that each bolt applies to the block of rock. These forces depend on the mechanical parameters governing the bolt-rock interaction, which are difficult to evaluate. In this work, specific numerical analyzes of great detail have been developed, able of evaluating the bolt-rock interaction (in shear and perpendicular to the interface that separates them) for numerous cases that were obtained by varying the main geometric parameters of the bolt, the mechanical properties of the binder material and rock. Thanks to this complex study, it was possible to describe the variability of the interaction parameters and to define, through graphs, the trend of the stabilization forces as the main geometric and mechanical parameters that can be encountered in practice change. The graphs obtained are a useful tool for the correct design of fully geouted passive bolts and the stabilization of potentially unstable rock blocks on the walls of underground cavities or on the faces of surface excavations.

Key words: passive bolt, cement grout, rock block stabilization, rock reinforcement, bolt-rock interaction; stabilizing forces

Nomenclature

E_{binder}	Elastic modulus of the material constituting the annular binder
E_{rock}	Elastic modulus of rock
$(EA)_{bolt}$	axial bolt stifness
$(EJ)_{bolt}$	flexural bolt stiffness
k	stiffness of the normal interaction springs
L_a	length of the bolt section that crosses the potentially unstable block
L_p	length of the bolt section in the stable rock (anchoring length)
$N_{0,max}$	axial stabilizing force that the bolt applies to the rock block
N_{slip}	force for a unit bolt length which causes the bolt-rock interface to fail
N_{test}	applied axial force at the bolt head during a slip test
N_{yield}	force causing the steel bar failure under a tensile stress
t_{binder}:	thickness of the binder annulus
$T_{0,max}$	transversal stabilizing forces that the bolt applies to the rock block (perpendicular to the bolt axis, directed upward, in the plane of the bolt axis and the block displacement vector)
T_{test}	transversal force applied to the bolt head during an in situ test
v	relative axial displacement between the bolt and the surrounding rock
y	transversal displacement of the bolt (against the surrounding rock) as it undergoes deformation due to the movement of the block

α	parameter characterising the rock-bolt interaction in the axial direction between the bolt and the surrounding rock $\alpha = \sqrt{\frac{\beta_c \cdot P_{hol}}{EA}}$
β	parameter characterizing the rock-bolt interaction in the transversal direction between the bolt and the surrounding rock $\beta = \sqrt[4]{\frac{k \cdot \Phi_{hole}}{4 \cdot EJ}}$
β_c	stiffness of the shear interaction springs at the bolt-rock interface
δ	displacement vector of the rock block (parallel to the slip surface)
$\delta_{ax,test}$	measured axial displacement of the bolt head
$\delta_{tr,test}$	measured transversal displacement of the bolt head
Φ_{bar}	diameter of the steel bar
Φ_{hole}	diameter of the hole (of the bolt)
σ	normal stress (perpendicular) to the outer surface of the bolt
τ	shear stress that exists at the rock-bolt interface
ϑ	angle which forms the displacement vector of the block δ with the direction of the bolt axis

Introduction

Passive bolts have long been employed in geotechnical engineering to stabilize soils and rocks. A passive bolt is made up of a bar that is placed into a borehole that is dug into the soil or rock mass nearby and fastened to it with a cementitious or resin-based injection. According to Windsor and Thompson (1993), 1) the rock or soil, 2) the reinforcing bar, 3) the internal fixture to the borehole wall, and 4) the exterior fixture to the excavation surface are the four main parts of a rock bolt reinforcement system. For example, by eliminating joint movements and pushing the rock mass to maintain itself, the rock bolting system in particular may increase the competency of disturbed rock masses (Kaiser et al., 1992).

Tensile, compressive, shear, and bending stresses can be supported by fully grouted rock bolts, which have the ground's gap between the rod and the ground totally filled with a binding material. A debonding process that begins if the axial stress on the bar exceeds a certain value and spreads throughout the interface is thought to be the most likely place for fully grouted bolt failure, according to experience from around the world (e.g. Stillborg, 1994; Li and Stillborg, 1999; Moosavi et al., 2005). For instance, due to an increase in axial, shear, and bending moments in the bolt rod, a fully grouted bolt intersected by a joint may affect the shearing of a joint and increase bolt resistance (Ranjbarnia et al., 2016; Oreste & Dias, 2012). According to Lang (1961), rock bolts can be used to "lock together" blocks in highly fractured rock masses to form a "reinforced arch" around an underground aperture that can stabilize the hollow. Rock bolting significantly affects the rigidity of a jointed rock mass in addition to strengthening or stabilizing it (Chappell, 1989). Because they are simple to install, versatile, and relatively inexpensive compared to other options, rock bolts are frequently used to support jointed surrounding rock and reinforce the rock mass (Indraratna and Kaiser, 1990).

While for active bolts the tensile load transfers from the element as an active compressive load, increasing therefore the resulting stress confinement in the rock, for passive bolts the initial load on passive reinforcing parts is zero, and when the potentially unstable rock block is moved, transmit stabilizing forces and the mobilized stabilizing load rises until the block is fully stabilized (Carranza-Torres, 2009). It is crucial to consider the physical and mechanical properties of the binder, either cementitious or resin-based during the design phase of the bolt, because it interacts with the surrounding rock.

Cementitious and resin materials are typically used to secure the bolt within the hole, and this type of set up is known as Continuous Mechanically Coupled (CMC) elements. For cementitious binders, a common water to cement (w/c) ratio is between 0.35 and 0.5, and the grout should be easily pumpable without being overly fluid (Kilic et al., 2002; Bawden, 2011). As for resin-based binders, a plastic cartridge containing two components (i.e. a resin and catalyst in separate compartments) is inserted in the drilled hole ahead of the bolt element (Bawden, 2011). Epoxy resins, silicate resins, polyester resins, and polyurethane resins are examples of common forms of resin. The catalyst and resin are mixed via an exothermic reaction as the cartridge is spun into the hole. Depending on the mix requirements, the resin sets in 20 seconds to 3 minutes, forming a solid anchor. Aldrian et al. (2019) claim however that very little grout can enter the surrounding cracks because the cartridge capacity is fixed and the inserted steel is creating only the "pressure" necessary to completely fill the annular gap.

Numerous laboratory and field studies have been conducted to examine the behavior of the rock-bolt grouted system. Pull-out tests (tension loading) or shear tests (shear loading) can be used to test the load capacity of bolt in the field or the lab. Standards like DIN-21521 (1990) or ISRM recommendations for rock bolt testing should be followed while conducting rock bolt tests. There are three primary failure scenarios in the event of a grouted anchor in

111 the bedrock or concrete: failure of the rod, rock failure and failure at the interface rock/grout
112 or steel grout. The failure mode is frequently a rock failure for cases with minor embedment
113 depths where the embedment depth is between three and five times the diameter of the bolt
114 (Ljungberg 2016).

115 According to Gambarova (1981) and Li and Stillborg (1999), adhesion, mechanical interlock,
116 and friction made up the majority of the interfacial bond strength under the pullout test. Kilic
117 et al. (2002) concluded that the mechanical properties of the grouting materials, which can
118 be altered by the water to cement ratio, mixing time, additives, and curing time, are mostly
119 what determine the bolt capacity. The bolt bearing capacity improves with increasing bolt
120 diameter and length, which is limited to the ultimate tensile strength of the bolt materials.
121 Craig and Murnane (2013) tested polyurethane-based resin binders with bolts with the scope
122 of accelerating ground support activities. Li et al. (2016) observed that the unconfined
123 compressive strength (UCS) of the grout and bond strength are linearly related. As long as
124 the bolt shank's yield strain is not excessively high, the bond strength of the rock bolt—that
125 is, the average shear stress at the bolt-grout interface when the bolt begins to slide along
126 the interface—seems to rise with embedment length instead of remaining parameters.

127 Chen et al. (2017) observed that the bonding capacity from pull-out tests in the unconfined
128 situation grew linearly with sample diameter up to 356 mm before remaining constant after
129 that. The bonding capacity, however, increased linearly with sample diameter up to 300 mm
130 in confined conditions. After that, it seemed like bonding capability peaked. Additionally, the
131 bonding capacity was always greater in the restricted setting than it was in the unconfined
132 one. Similar results were obtained by Moosavi et al. (2002).

133 Li et al. (2017) observed that the pullout strength of a rock bolt is somewhat influenced by
134 their temperatures. Temperature improves the pullout strength for temperatures between
135 20°C and 35°C. Temperature causes a decrease in pullout strength at temperatures

between 50°C and 70°C. Salcher and Bertuzzi (2018) performed in situ pull-out test in an Australian sandstone, with a cementitious and resin binder. Cement-grouted bolts consistently performed in a stiff manner. It was demonstrated that rock bolts cement-grouted in large diameter shale holes produced the least stiff results as well as the stiffest outcomes. Shale resin bolts had more constant behavior. In shale, one may use cement-grouted bolts in holes of a large diameter if a great rigidity is desired. The pull test findings showed no correlation between bolt performance and resin annulus width. Bajwa et al (2017), comparing grout and resin binders, observed that in small borehole the cementitious grouted bolts achieved higher peak pull-out load in comparison with resin-grouted bolts, whereas for larger boreholes the contrary was true. Aziz et al. (2018) evaluated the shear performance of various pretensioned fully grouted cable bolts using a novel experimental single shear testing technique. 19 single shear tests were performed to examine the effects of the bolt type, surface profile type, pretension load, structure, bonding and debonding, and failure modes. Comparing plain strand cable bolts to rough surface strand cables, it was discovered that plain strand cable bolts debonded more easily for the same length of the cable encapsulated in the host material. Spagnoli et al. (2021) presented promising data about the mechanical properties of polyurea silicate with a true thixotropic behavior and pull-out test results on anchors (rebars and hollow). About the half of tests ended up with the failure of the bar rather than through an interface failure bolt/resin.

In this paper, the mechanical behavior of fully grouted passive bolts for the stabilization of potentially unstable rock blocks on underground cavity walls or surface rock faces is analyzed in detail. Some simplified equations (Oreste and Spagnoli, 2020) allow to determine the stabilization forces of the bolt, on the basis of different geometric and mechanical parameters. Two of these are of great importance because they are able to describe the bolt-rock interaction in the axial and transverse directions. Unfortunately, these interaction parameters are difficult to evaluate, even by resorting to specific in situ tests. A

detailed analysis through numerical modeling has made it possible to obtain these parameters with a certain precision. Several cases have been considered, varying the characteristics of the bolt and the rock, in a typical field of variability that can be encountered in practice. The developed study allows to define the interaction parameters for different types of bolt and rock and thus arrive at a quick evaluation of the stabilizing forces of the bolt, a fundamental step for the design phase.

Simplified equations and required parameters to analyse the stabilizing contribution of a passive bolt to a rock block

The analysis of the interaction between the fully grouted passive bolt and the surrounding rock, was carried out by Oreste and Cravero (2008), Oreste (2009a; 2009b), Ranjbarnia et al. (2014), Oreste and Spagnoli (2020). It it possible to identify the stabilizing forces that the single bolt applies to a potentially unstable block of rock, which tends to move (even with very small displacement values) along a sliding surface (Fig. 1). This analysis is based on the assumption that the reaction of the rock to the displacements of the bolt can be represented with independent springs (Winkler springs), capable of manifesting reaction forces as a function of the relative displacements of each point of the bolt with respect to the surrounding rock. The following hypotheses were considered:

- The bolt (steel bar and binder annulus) is represented by a one-dimensional linear element, i.e. characterized only by the length and by the axial $(EA)_{bolt}$ and bending $(EJ)_{bolt}$ stifness;
- Two different zones of the bolt are identified, the crossing zone of the potentially unstable block L_a and the anchorage length in the stable rock portion L_p, beyond the potentially unstable block; the intersection of the bolt with the internal surface of the block allows to identify the point 0, which separates the crossing area from the

anchoring area and divides the total length of the bolt into two parts of length L_a and L_p;

- Each point of the bolt is connected to the surrounding rock through two different Winkler springs, one normal (perpendicular to the bolt) and the other parallel to it; the first allows to consider the normal reaction of the rock to the transversal displacements of the bolt, the second the shear reaction to the axial (relative) displacements on the bolt-rock interface;
- The displacement of the rock block in the direction of the slip surface deforms the bolt and activates the reaction of the rock around it, as foreseen by the interaction springs; as the displacement of the block increases, the stresses along the bolt also increase;
- Upon reaching the limit operating condition of the bolt, when the approach to failure of the steel bar or of the connection of the bolt to the surrounding rock occurs, in correspondence with a certain value of the displacement of the block, the maximum static contribution offered by the bolt to the block stabilization occurs.

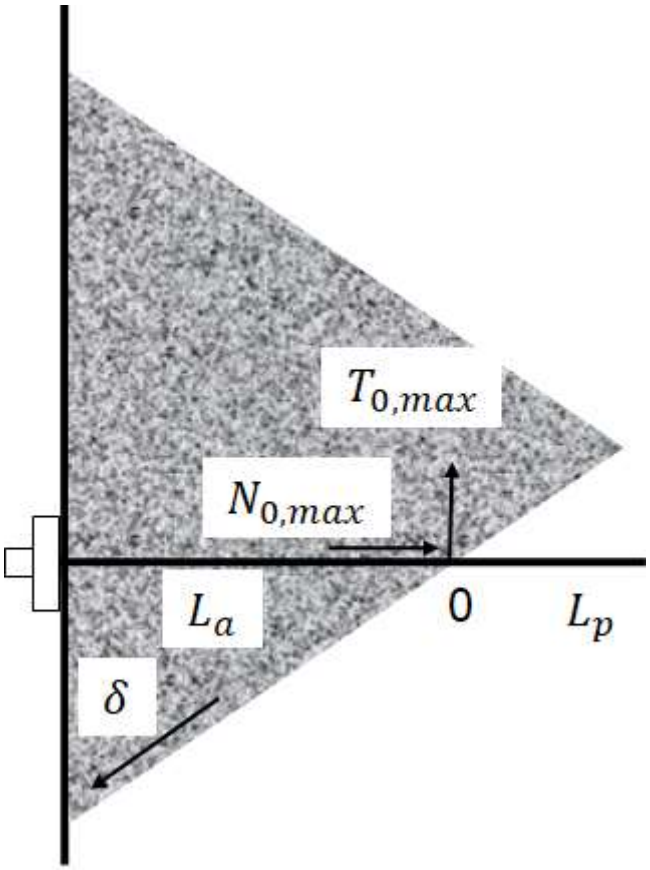

Fig. 1 Diagram of a potentially unstable block of rock in presence of a fully cemented passive bolt. Key: L_a and L_p are respectively the lengths of the bolt section that crosses the potentially unstable rock block, and of anchorage in the stable rock; δ is the displacement vector of the block (parallel to the slip surface); $N_{0,max}$ and $T_{0,max}$ are the stabilizing forces that the bolt applies to the block of rock.

The maximum stabilization forces offered by the bolt to the potentially unstable block of rock, in the limit operating condition, are the forces that must be considered to design of the bolting intervention, i.e. to define the number and diameter of the bolts necessary to stabilize a rock block. The stabilization forces offered by the single bolt are two, one is directed in the axial direction of the bolt ($N_{0,max}$), and the other one ($T_{0,max}$) is directed in a perpendicular direction to the bolt, in a plane which includes both the bolt and the displacement vector of the block (δ).

Oreste and Spagnoli (2020) have identified some simplified equations capable of providing the stabilizing forces that a fully cemented passive bolt is able to apply to a potentially unstable block of rock. This study is based on an extensive parametric analysis, varying all the main input data (geometric and mechanical) that influence the bolt-rock interaction problem:

$$N_{0,max} = min\left(\frac{N_{yield}}{F_{s,adm,yield}} \cdot \frac{\xi \cdot \left(1+e^{-2\alpha L_a}\right)}{\chi \cdot tan(\vartheta)+\xi \cdot \eta}\ ;\ \frac{N_{slip}}{F_{s,adm,slip}} \cdot \frac{\omega}{\alpha}\right) \quad (1)$$

$$T_{0,max} = min\left(\frac{N_{yield}}{F_{s,adm,yield}} \cdot \frac{\rho}{\chi+\frac{\xi}{tan(\vartheta)} \cdot \eta}\ ; \frac{N_{slip}}{F_{s,adm,slip}} \cdot \frac{2 \cdot tan(\vartheta)}{\lambda \cdot \psi \cdot \alpha}\right) \quad (2)$$

Where N_{yield} is the force causing bar failure under a tensile stress $N_{yield} = \sigma_{yield} \cdot A_{bar}$; N_{slip} is the force which causes the bolt-rock interface to fail for a unit bolt length $N_{slip} = \tau_{lim} \cdot \pi \cdot \Phi_{hole}$; $(EA)_{bolt}$ is the axial stiffness of the bolt, considering both the steel bar and the binder annulus, i.e. $(EA)_{bolt} = E_{st} \cdot \left(\frac{\pi}{4} \cdot {\Phi_{bar}}^2\right) + E_{binder} \cdot \left[\frac{\pi}{4} \cdot \left({\Phi_{hole}}^2 - {\Phi_{bar}}^2\right)\right]$; $(EJ)_{bolt}$ is the bending stiffness of the bolt, considering both the steel bar and the binder annulus, i.e. $(EJ)_{bolt} = E_{st} \cdot \left(\frac{\pi}{64} \cdot {\Phi_{bar}}^4\right) + E_{binder} \cdot \left[\frac{\pi}{64}\left({\Phi_{hole}}^4 - {\Phi_{bar}}^4\right)\right]$; $\alpha = \sqrt{\frac{\beta_c \cdot \pi \cdot \Phi_{hole}}{(EA)_{bolt}}}$; $\beta = \sqrt[4]{\frac{k \cdot \Phi_{hole}}{4 \cdot (EJ)_{bolt}}}$; $\lambda = \left[\frac{(EA)_{bolt} \cdot \alpha}{(EJ)_{bolt} \cdot \beta^3}\right]$; $\xi = 2 \cdot (EA)_{bolt} \cdot \alpha \cdot \Phi_{bar} \cdot (1 - e^{-2\alpha L_p})$; $\chi = 16 \cdot \sqrt{2} \cdot \left(1 + e^{-2\alpha\left(L_a+L_p\right)}\right) \cdot (EJ)_{bolt} \cdot \beta^2 \cdot e^{-\frac{\pi}{4}}$; $\eta = \left(e^{-2\alpha L_a} \cdot e^{\alpha \cdot \frac{\pi}{4 \cdot \beta}} + e^{-\alpha \cdot \frac{\pi}{4 \cdot \beta}}\right)$; $\varrho = 4 \cdot (EJ)_{bolt} \cdot \beta^3 \cdot \Phi_{bar} \cdot \left(1 + e^{-2\alpha\left(L_a+L_p\right)}\right)$; $\psi = \left[\frac{\left(1+e^{-2\alpha L_a}\right) \cdot \left(1+e^{-2\alpha L_p}\right)}{\left(1+e^{-2\alpha\left(L_a+L_p\right)}\right)}\right]$ and $\omega = \left[\frac{\left(1-e^{-2\alpha L_p}\right)}{\left(1+e^{-2\alpha L_p}\right)}\right]$.

Two fundamental parameters condition the values of the stabilization forces $N_{0,max}$ and $T_{0,max}$ (Figure 2), i.e. β_c and k; which represent respectively the stiffness of the shear interaction springs at the bolt-rock interface and the stiffness of the normal interaction springs.

$$\tau = \beta_c \cdot v \quad (3)$$

where τ is the shear stress that exists at the rock-bolt interface, and v is the relative axial displacement between the bolt and the surrounding rock.

$$\sigma = k \cdot y \quad (4)$$

where σ is the normal (perpendicular) stress applied to the outer surface of the bolt, and y is the transverse displacement of the bolt (against the rock) as it undergoes deformation due to the movement of the block.

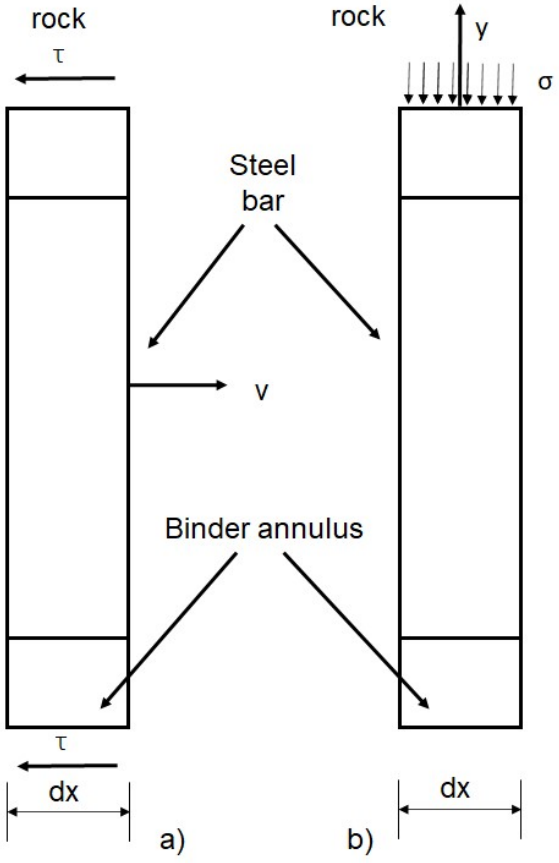

Figure 2. Representation of the stresses applied by the rock (τ and σ) on the external surface of an infinitesimal element of a dx bolt following the relative displacements (v and y) of the bolt. Key: a) represents the shear interaction; b) represents the normal interaction (perpendicular to the bolt); τ is the shear stress applied by the rock on the external surface of the bolt; σ is normal stress applied by the rock on the external surface of the bolt.

Parameters β_c and k describe the rock response during the bolt deformation. They depend on the elastic modulus of the rock, on the geometry of the bolt (diameter of the bar, thickness of the binder annulus) and on the elastic modulus of the steel and the binder material. In situ tests on test bolts (Figure 3) can help in estimating β_c and k starting from the applied forces and the measurement of the induced displacements, but unfortunately in general there are very high forces applied on the bolt head and relatively small displacements. The reduced precision and errors in the measurement of the displacements of the bolt head can lead to large uncertainties on the two parameters which are fundamental for obtaining a reliable estimate of the stabilizing forces $N_{0,max}$ and $T_{0,max}$.

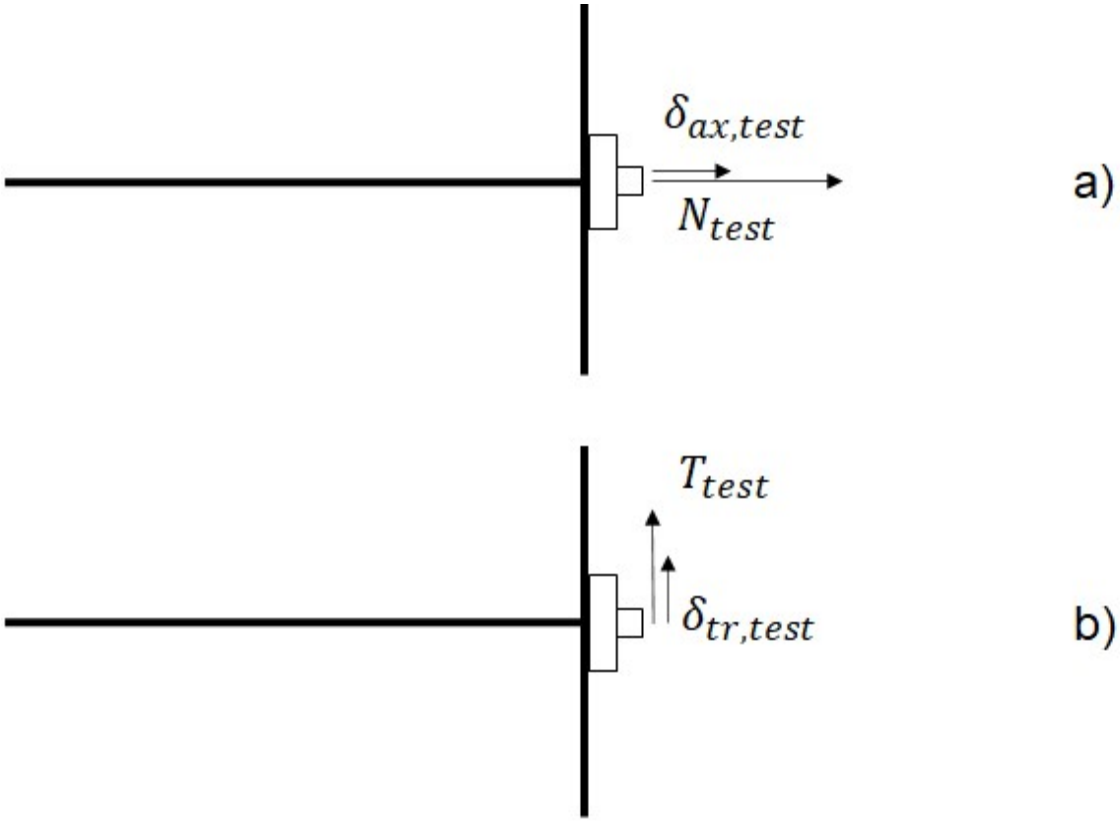

Figure 3. In situ tests on test bolts for the determination of the parameters β_c and k. Key: a) is the pull-out test with application of an axial force to the bolt head; b) is the shear test with application of a transversal force to the bolt head; N_{test} is the applied axial force; T_{test} is the applied transversal force; $\delta_{ax,test}$ is the measured axial displacement of the bolt head; $\delta_{tr,test}$ is the measured transverse displacement of the bolt head.

More specifically, from in situ tests it is possible to determine the parameters β_c and k using the following two equations:

$$\delta_{ax,test} = \frac{N_{test}}{(EA)_{bolt}\cdot\sqrt{\frac{\beta_c\cdot\pi\cdot\Phi_{hole}}{(EA)_{bolt}}}} \cdot \frac{\left(1+e^{2\cdot\sqrt{\frac{\beta_c\cdot\pi\cdot\Phi_{hole}}{(EA)_{bolt}}}\cdot L_{test}}\right)}{\left(1-e^{2\cdot\sqrt{\frac{\beta_c\cdot\pi\cdot\Phi_{hole}}{(EA)_{bolt}}}\cdot L_{test}}\right)} \quad (4)$$

$$k = \left(\frac{T_{test}}{2\cdot(EJ)_{bolt}\cdot\delta_{tr,test}}\right)^{\frac{4}{3}} \cdot \frac{4\cdot(EJ)_{bolt}}{\Phi_{hole}} \quad (5)$$

To obtain β_c from equation 4 it is necessary to resort to a numerical solution.

The analysis of the bolt-rock interaction through numerical modeling

It is possible to analyze in detail the complex interaction between the fully cemented passive bolt and the surrounding rock thanks to numerical modelling. More specifically, through two-dimensional numerical modeling, the axial interaction (in the axisymmetric configuration) and the transverse interaction (in a cross section of the bolt) can be simulated.

In this work the calculation code FLAC 2D ver 8.1 of the Itasca Company was used. This code is able to solve the stress-strain problem through a finite difference solution. In the first case, after applying an axial force N_{test} to the bolt head, the displacement of the bolt head $\delta_{ax,test}$ can be determined as a result of the calculation. Based on the pair of values N_{test}-$\delta_{ax,test}$, β_c can be determined (equation 4).

Figure 4 shows the detail of the numerical model developed to analyze the axial interaction of the bolt; in this model, only half of the bolt and the surrounding rock is represented, exploiting the axisymmetric symmetry of the problem (vertical y-axis represents the axis of

283 the steel bar). The model allows the study of the axial interaction with great precision and
284 has the following main characteristics:

285 • Total number of elements: 60000
286 • Thickness of the rock considered around the bolt: 1.5 m
287 • Length of the bolt simulated in the model: 2 m
288 • Overall length of the model in the axial direction of the bolt: 4 m
289 • Number of elements dedicated to the semi-section of the steel bar: 8
290 • Number of elements dedicated to the annular binder: 4

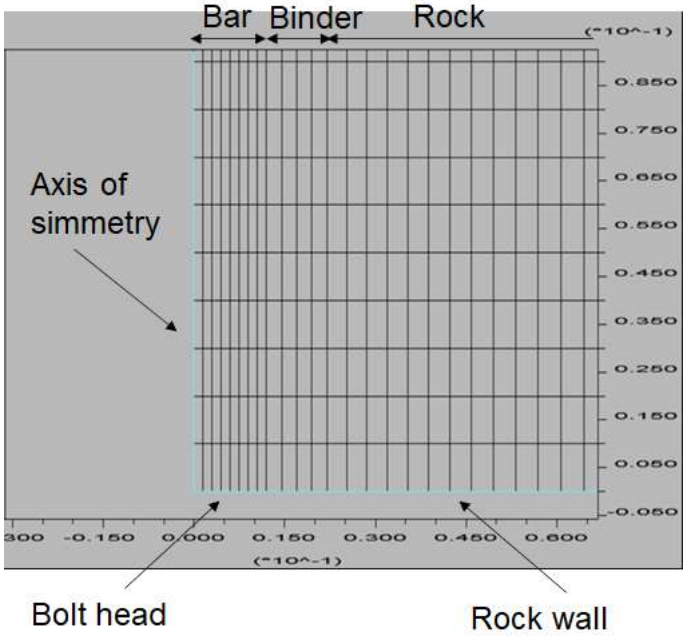

291

292 Figure 4. Detail of the two-dimensional axisymmetric numerical model developed to study the axial
293 interaction between the bolt and the surrounding rock. Key: the left edge represents the axis of
294 symmetry of the bolt, the lower one the rock face where the head of the bolt is located; the first 8
295 elements represent half of the steel bar in the analyzed section, the next 4 the annular binder that
296 connects the steel bar to the surrounding rock.

297

Different values of the diameter of the steel bar, of the thickness of the annular binder, of the elastic models of the rock and of the material that constitutes the annular binder were analysed:

- Diameter of the steel bar Φ_{bar}: 24 mm and 32 mm
- Thickness of the annular binder t_{binder}: 10 mm and 15 mm
- Elastic modulus of rock E_{rock}: 20 GPa, 60 GPa, 100 GPa
- Elastic modulus of the material constituting the annular binder E_{binder}: 2 GPa and 8 GPa

The considered cases, 24 in total, allow us to investigate the axial interaction of the bolt for all possible cases that may arise in reality when passive bolting (fully grouted) is adopted in rock masses. More specifically, a bar with a small diameter (24 mm) and a large diameter (32 mm), a reduced (10 mm) and high (15 mm) thickness of the annular binder, a rock with low (20 GPa), intermediate (60 GPa) and high (100 GPa) mechanical characteristics, a material constituting the binder having an elastic modulus 2 GPa (resin) and 8 GPa (traditional cementitious grout) were considered.

For each of the 24 cases analyzed it was possible to determine the parameter β_c. Figure 5 shows the graph that allows to synthetically represent the values calculated on the basis of the results of the numerical modeling.

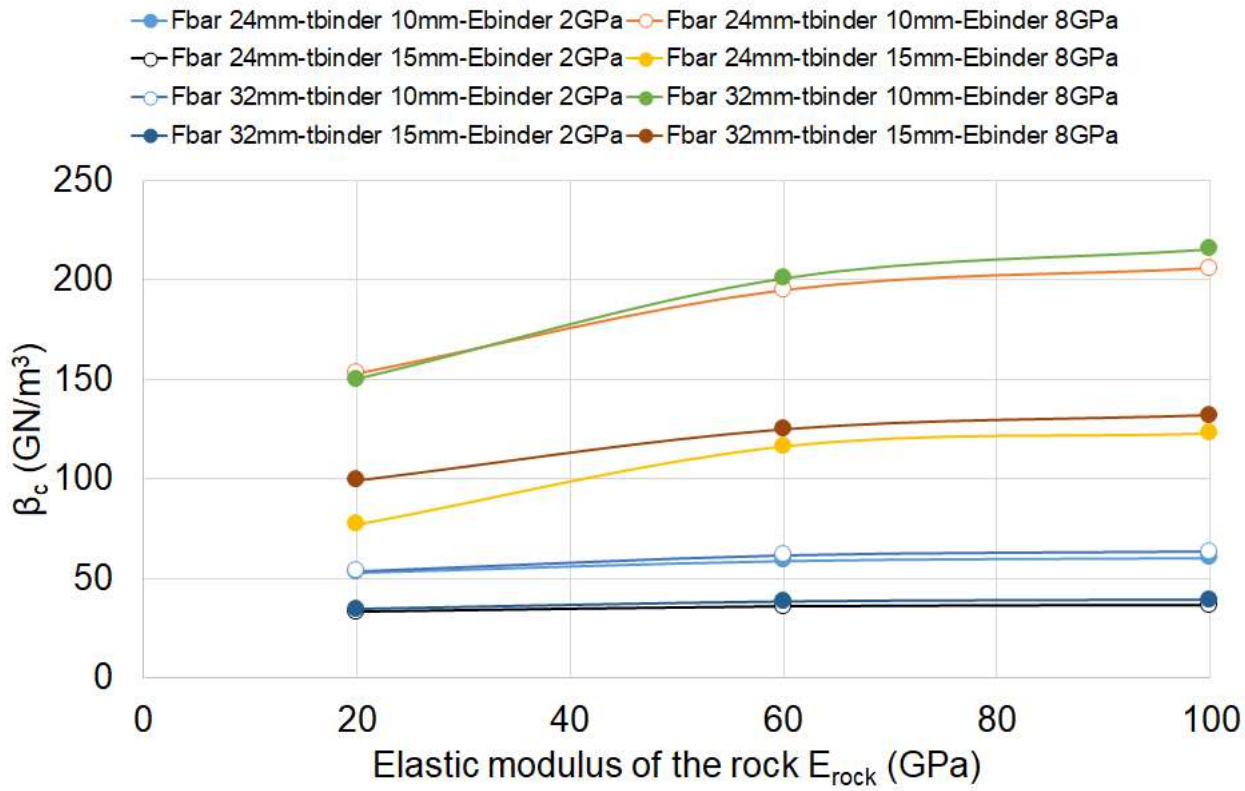

317

318 Figure 5. Trend of the parameter β_c, which governs the axial interaction of the passive bolt,
319 as the elastic modulus of the rock varies, for different combinations of the diameter of the
320 bar (Φ_{bar}), the thickness of the binder (t_{binder}), the elastic of the material that constitutes
321 the binder (E_{binder}).

322 From the analysis of Figure 5, the following observations can be made:

323 • The diameter of the bar has, in general, a small influence on the axial interaction
324 parameter β_c, with the sole exception of the case of weak rock, high thickness of the
325 annular binder and bar-rock connection with traditional cementitious grout (in this case
326 β_c increases by about 30% when going from a small (24 mm) to a large (32 mm) bar
327 diameter. In the case of using the resin as a bolt-rock connection material, the stiffness
328 of the rock has no effect on the axial interaction parameter β_c

- The thickness t_{binder} of the annular binder has an important effect on the interaction parameter β_c: as it decreases from 15 mm to 10 mm, β_c increases considerably by 60-65%, mostly with the use of traditional cementitious grout
- With the use of traditional cementitious grout (E_{binder}=8 GPa) there are no significant increases in β_c for values of the elastic modulus of the rock E_{rock} above 60 GPa; for lower values of the elastic modulus of the rock (E_{rock}=20÷60 GPa) β_c grows considerably with E_{rock}.

The results, therefore, can be summarized as follows. In the case of using resins for the bar-rock connection, β_c essentially depends on the thickness t_{binder}:

$\beta_c \cong 103.3 - 4.48 \cdot t_{binder}$ (with β_c expressed in GN/m^3 and t_{binder} in mm) (6)

In the case of using traditional cementitious grout, β_c depends on both E_{rock} and t_{binder}:

$\beta_c \cong (277.5 - 15 \cdot t_{binder}) + 1.125 \cdot E_{rock}$ (with β_c expressed in GN/m^3, t_{binder} in mm and E_{rock} in GPa, for E_{rock}≤60 GPa) (7)

In the latter equation (for traditional cementitious grout), in the only case of weak rock (E_{rock}≤=20 GPa) and high thickness of the annular binder (t_{binder}=15 mm), β_c must be increased by 15% when considering a intermediate diameter steel bar (28 mm) and 30% for large diameter bar (32 mm). Furthermore, for E_{rock} greater than 60 GPa (rock with high mechanical characteristics), the values of β_c calculated for E_{rock}=60 GPa can be adopted without making significant errors.

As regards the transverse interaction, a two-dimensional numerical model of the cross section of the bolt has been developed; after applying a shear force T_{test} to the bolt (at the center of the steel bar), the displacement of the bar axis $\delta_{tr,test}$ was calculated. The pairs of values T_{test}-$\delta_{tr,test}$ then allow to determine the interaction parameter k (equation 5).

Figure 6 shows the detail of the numerical model used, which considers the entire cross section of the bolt and the surrounding rock. It is able to analyze in great detail the transversal interaction of the bolt and has the following main characteristics:

- Total number of elements: 200000
- Thickness of the rock considered around the bolt: 0.5 m
- Average dimension of each numeric element: 1.5 mm x 1.5 mm; 14/19 numerical elements were used to simulate the steel bar along its diameter (Φ_{bar}=24/32 mm); 6/9 numerical elements have been used to represent the binder annulus along its thickness (t_{binder}=10/15 mm)

The same 24 cases considered in the analysis of the axial interaction were analyzed also in the transversal one, by varying the diameter of the bar, the thickness of the binder around it, the elastic modulus of the rock and the elastic modulus of the binder. The obtained results of the numerical calculation have been summarized in Figure 7.

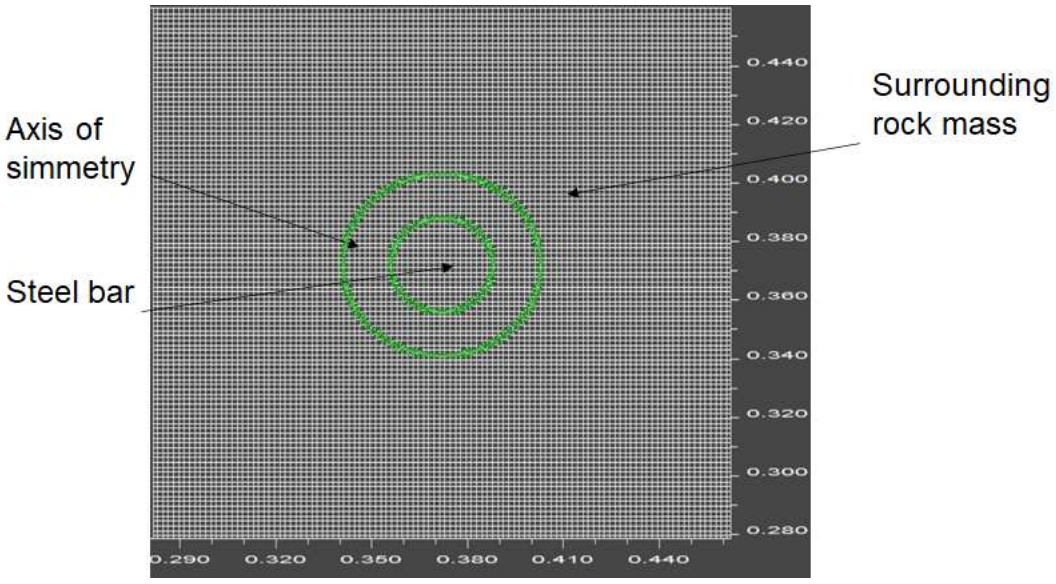

Figure 6. Detail of the two-dimensional transversal numerical model developed to study the transversal interaction between the bolt and the surrounding rock. The average size of the numerical elements used is 1.5 mm x 1.5 mm.

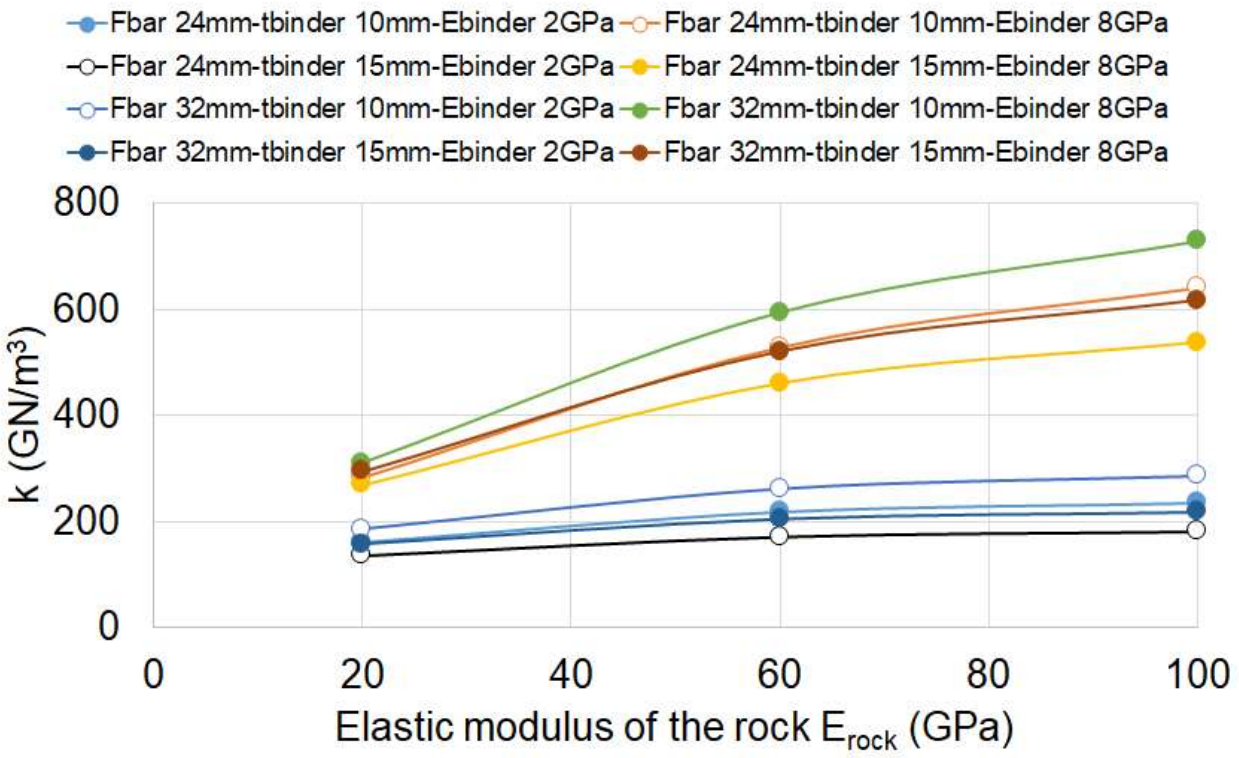

Figure 7. Trend of the parameter k, which governs the transversal interaction of the passive bolt, as the elastic modulus of the rock varies, for different combinations of the diameter of the bar (Φ_{bar}), the thickness of the binder (t_{binder}), the elastic of the material that constitutes the binder (E_{binder}).

From the analysis of Figure 7, the following comments can be made:

- The parameter k tends to grow with E_{rock} according to a parabolic trend (the influence of E_{rock} is greater for traditional cementitious grout, E_{binder}=8 GPa, less for resins, E_{binder}=2 GPa)
- The values of k are 2÷3 times greater when the binder is made up of traditional cementitious grout compared to the case of a binder made up of resins
- k tends to increase as the diameter of the bar increases and the thickness of the binder decreases
- the influence of Φ_{bar} and t_{binder} on k depends on the rock's elastic modulus E_{rock}: it is smaller for low E_{rock}, it increases for high E_{rock}

For each type of binder (traditional cementitious grout or resin), thickness of the binder annulus (10 or 15 mm) and diameter of the bar (24 or 32 mm) considered, it was possible to obtain the equations of the parabola which best describes the results of the numerical calculation in terms of k (GN/m^3) as the elastic modulus of the rock E_{rock} (GPa) varies:

binder made of traditional cementitious grout:

Φ_{bar}=24 mm; t_{binder}=10 mm: $k \cong -0.04156 \cdot E_{rock}^2 + 9.450 \cdot E_{rock} + 111.625$ (8)

Φ_{bar}=24 mm; t_{binder}=15 mm: $k \cong -0.03594 \cdot E_{rock}^2 + 7.675 \cdot E_{rock} + 129.875$ (9)

Φ_{bar}=32 mm; t_{binder}=10 mm: $k \cong -0.04688 \cdot E_{rock}^2 + 10.875 \cdot E_{rock} + 111.250$ (10)

Φ_{bar}=32 mm; t_{binder}=15 mm: $k \cong -0.04063 \cdot E_{rock}^2 + 8.900 \cdot E_{rock} + 133.250$ (11)

binder made of resin:

Φ_{bar}=24 mm; t_{binder}=10 mm: $k \cong -0.01281 \cdot E_{rock}^2 + 2.475 \cdot E_{rock} + 116.625$ (12)

Φ_{bar}=24 mm; t_{binder}=15 mm: $k \cong -0.00813 \cdot E_{rock}^2 + 1.550 \cdot E_{rock} + 108.250$ (13)

Φ_{bar}=32 mm; t_{binder}=10 mm: $k \cong -0.01625 \cdot E_{rock}^2 + 3.200 \cdot E_{rock} + 128.500$ (14)

Φ_{bar}=32 mm; t_{binder}=15 mm: $k \cong -0.01094 \cdot E_{rock}^2 + 2.075 \cdot E_{rock} + 120.875$ (15)

Estimation of the stabilization forces produced by the passive bolt on the basis of the mechanical parameters of the bolt-rock interaction

Thanks to the results obtained from the numerical modeling and the determination of the mechanical parameters of bolt-rock interaction in the axial (β_c) and transversal (k) direction, it is possible to proceed to the estimation of the stabilization forces on the basis of equations 1 and 2 (Oreste and Spagnoli, 2020). More specifically, it is possible to have a reliable

406 estimate of the stabilization force acting in the axial direction ($N_{0,max}$) and transversal
407 upwards ($T_{0,max}$), acting perpendicularly to the bolt with a vector belonging to the plane
408 encompassing the bolt itself and the block displacement vector δ (Fig. 1).

409 The following Figures (8-13) show the values of $T_{0,max}$ and $N_{0,max}$ as the elastic modulus of
410 the rock E_{rock} varies, for traditional cementitious grout, (E_{binder}=8000 MPa) and resin
411 (E_{binder}=2000 MPa), in the cases of steel bar with diameter Φ_{bar} 20 and 32 mm and
412 thickness of the binder annulus t_{binder} of 10 and 15 mm. These graphs assume a fundamental
413 design role, allowing the correct design of the fully grouted passive bolts in the different
414 conditions that can be encountered in engineering practice, guaranteeing the stabilization
415 of the potentially unstable blocks of rock, quickly defining the characteristics and the number
416 of bolts that are necessary.

417 These graphs were obtained assuming the following parameters present in equations 1 and
418 2:

419 • Length of the bolt in the two areas L_a (block crossing area) and L_p (anchor length in
420 the stable rock behind the block): 2 m
421 • Elastic modulus of steel E_{steel}: 210 GPa
422 • Limit shear stress τ_{lim} at the bolt-rock interface: 2.5 MPa
423 • Steel yield strength σ_y: 450 MPa
424 • Safety factors considered as minimum admissible against yield failure of the steel bar
425 ($F_{s,\mathrm{adm,yield}}$) and pullout failure at the bolt-rock interface ($F_{s,\mathrm{adm,slip}}$): 1.3.

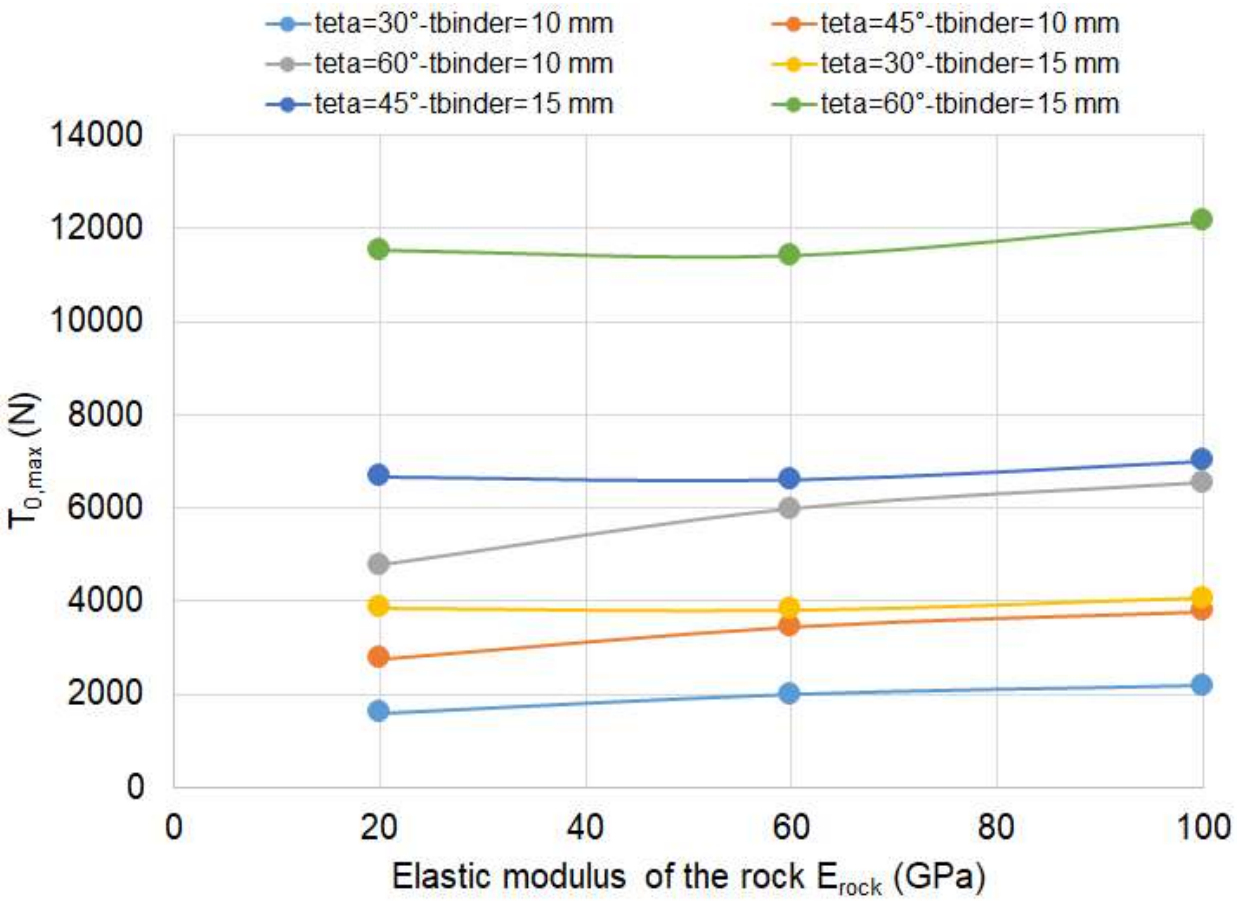

426

427 Figure 8. Trend of the transversal stabilization force $T_{0,max}$, as the elastic modulus of the
428 rock E_{rock} varies, for different combinations of the thickness of the binder annulus (t_{binder})
429 and of the angle ϑ which forms the displacement vector of the block δ with the direction of
430 the bolt axis. Case of a traditional cementitious binder (E_{binder}=8 GPa) and diameter of the
431 bar Φ_{bar}=24 mm.

432

433

434

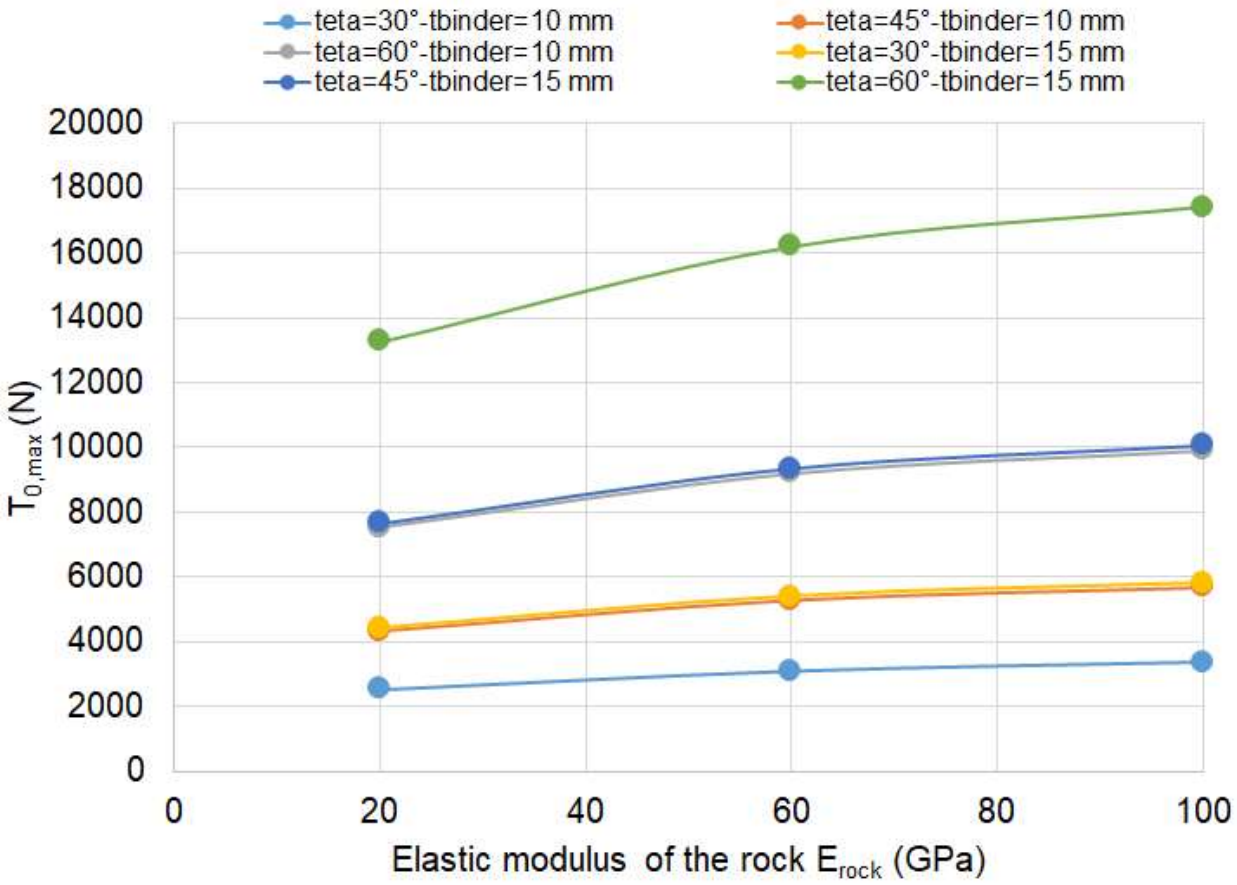

435

436 Figure 9. Trend of the transversal stabilization force $T_{0,max}$, as the elastic modulus of the
437 rock E_{rock} varies, for different combinations of the thickness of the binder annulus (t_{binder})
438 and of the angle ϑ which forms the displacement vector of the block δ with the direction of
439 the bolt axis. Case of a traditional cementitious binder (E_{binder}=8 GPa) and diameter of the
440 bar Φ_{bar}=32 mm.

441

442

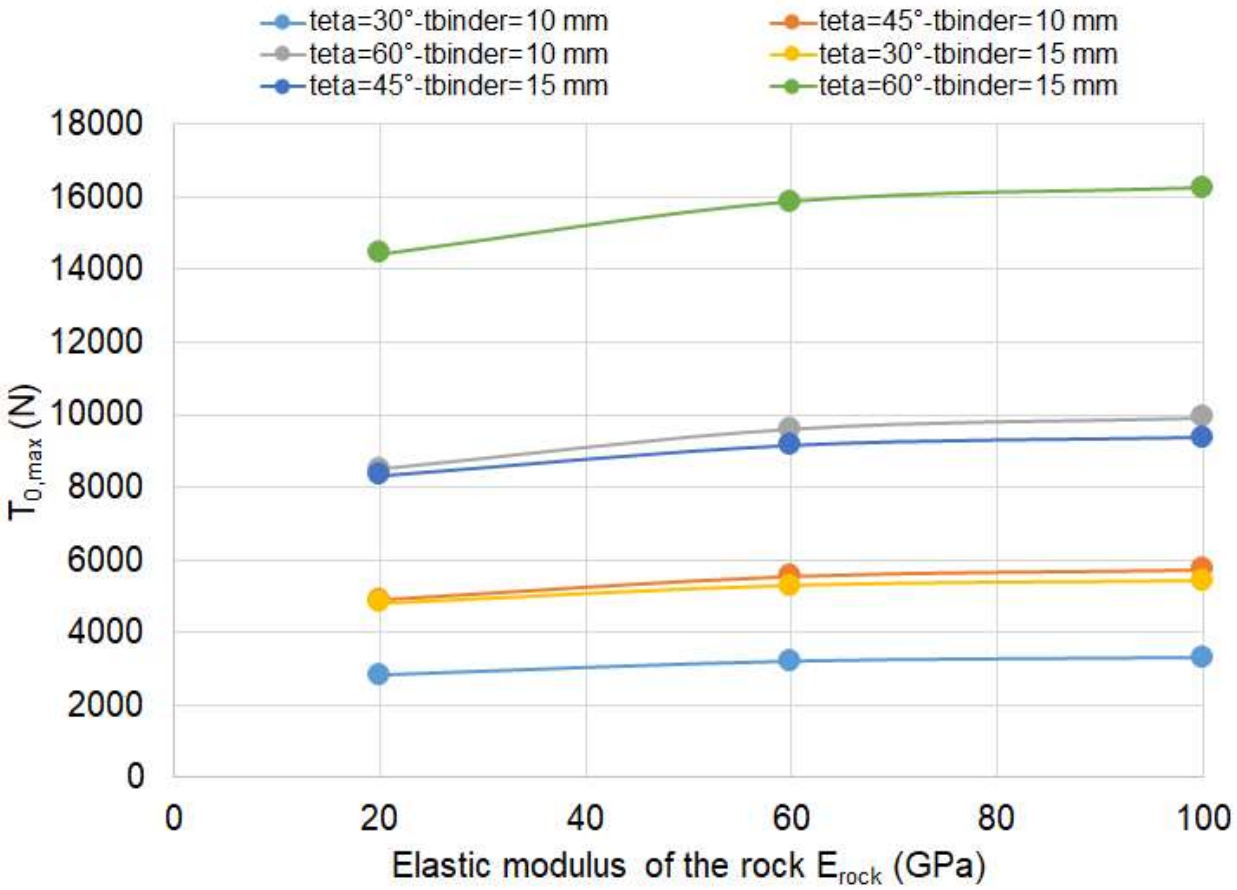

443

444 Figure 10. Trend of the transversal stabilization force $T_{0,max}$, as the elastic modulus of the
445 rock E_{rock} varies, for different combinations of the thickness of the binder annulus (t_{binder})
446 and of the angle ϑ which forms the displacement vector of the block δ with the direction of
447 the bolt axis. Case of a resin binder (E_{binder}=8 GPa) and diameter of the bar Φ_{bar}=24 mm.

448

449

450

451

452

453

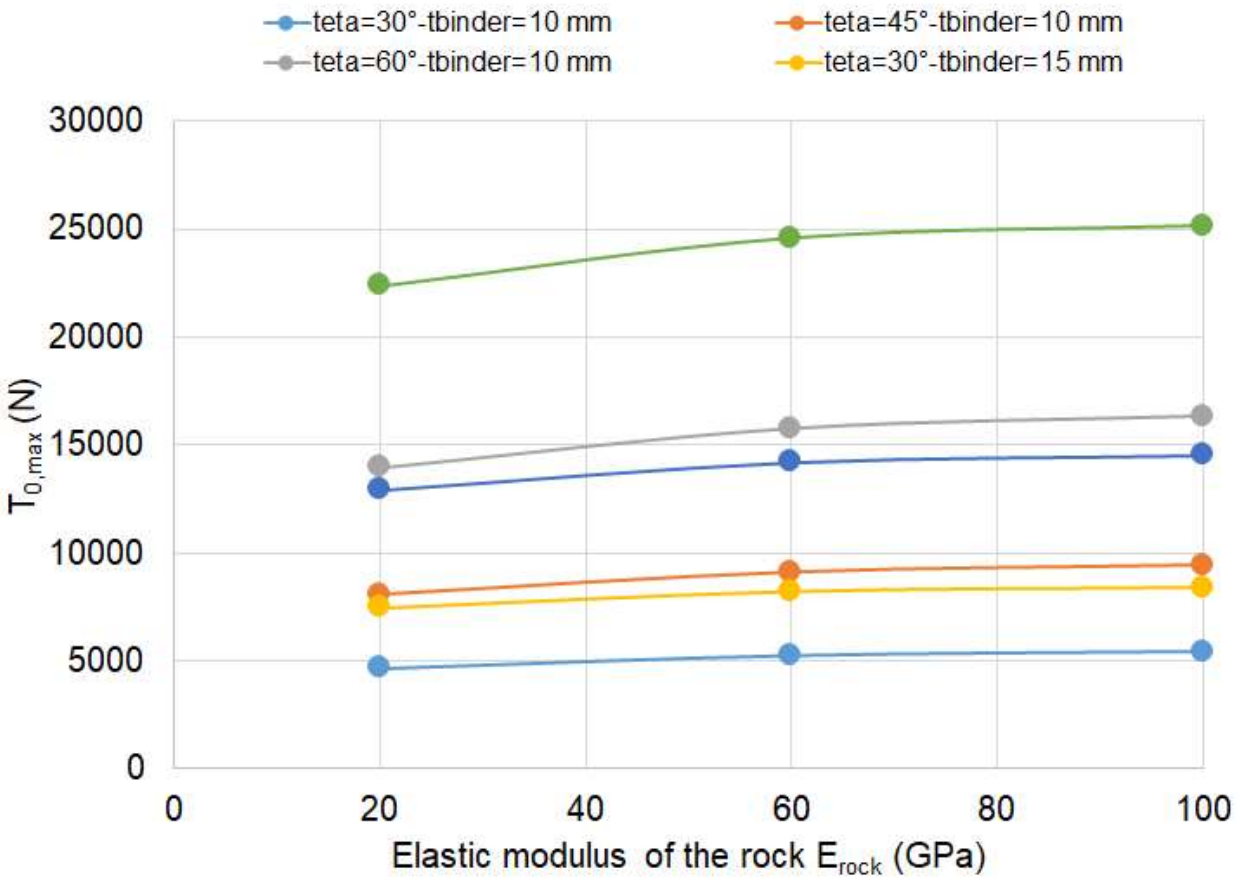

454

455 Figure 11. Trend of the transversal stabilization force $T_{0,max}$, as the elastic modulus of the
456 rock E_{rock} varies, for different combinations of the thickness of the binder annulus (t_{binder})
457 and of the angle ϑ which forms the displacement vector of the block δ with the direction of
458 the bolt axis. Case of a resin binder (E_{binder}=8 GPa) and diameter of the bar Φ_{bar}=32 mm.

459

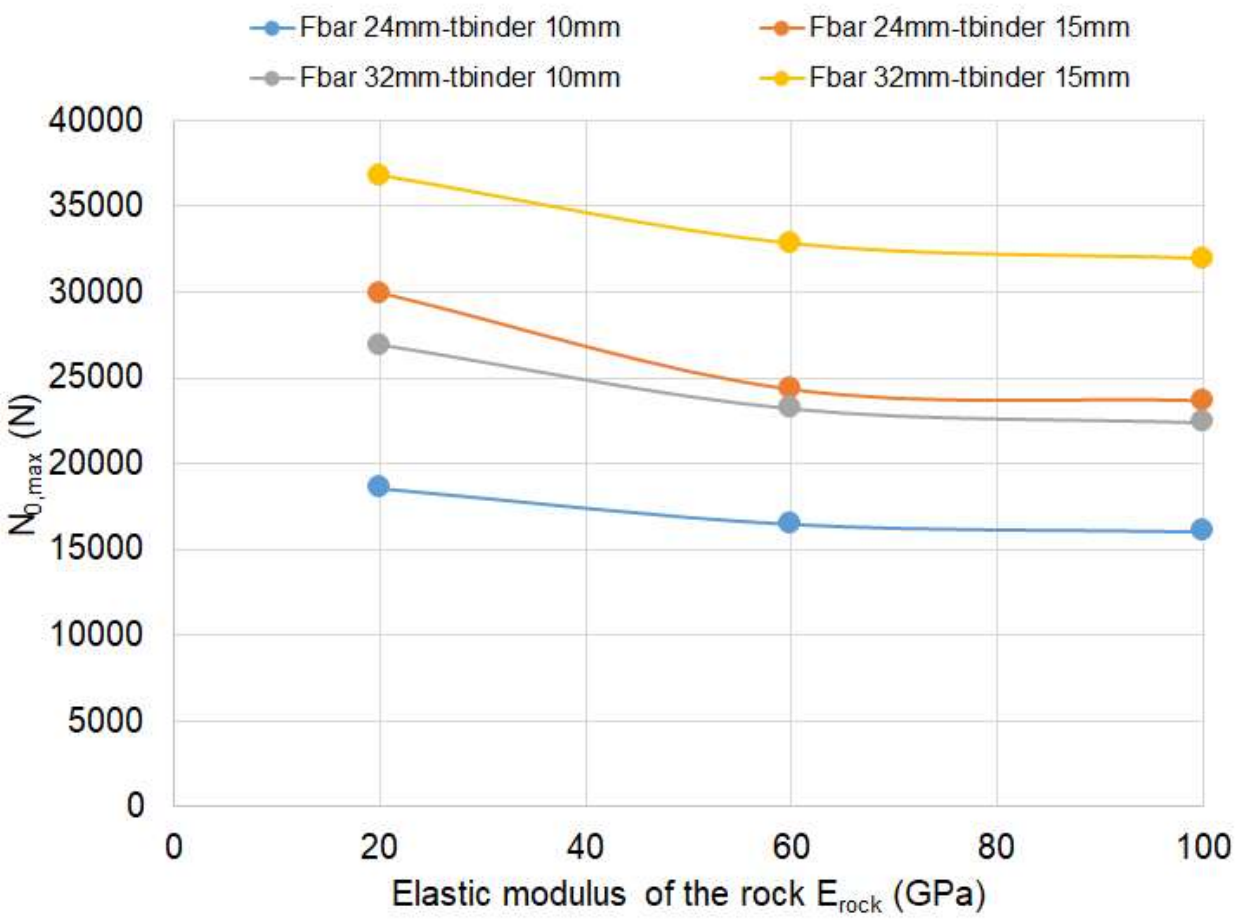

460

461 Figure 12. Trend of the axial stabilization force $N_{0,max}$, as the elastic modulus of the rock
462 E_{rock} varies, for different combinations of the thickness of the binder annulus (t_{binder}) and
463 of the angle ϑ which forms the displacement vector of the block δ with the direction of the
464 bolt axis. Case of a traditional cementitious grout (E_{binder}=8 GPa).

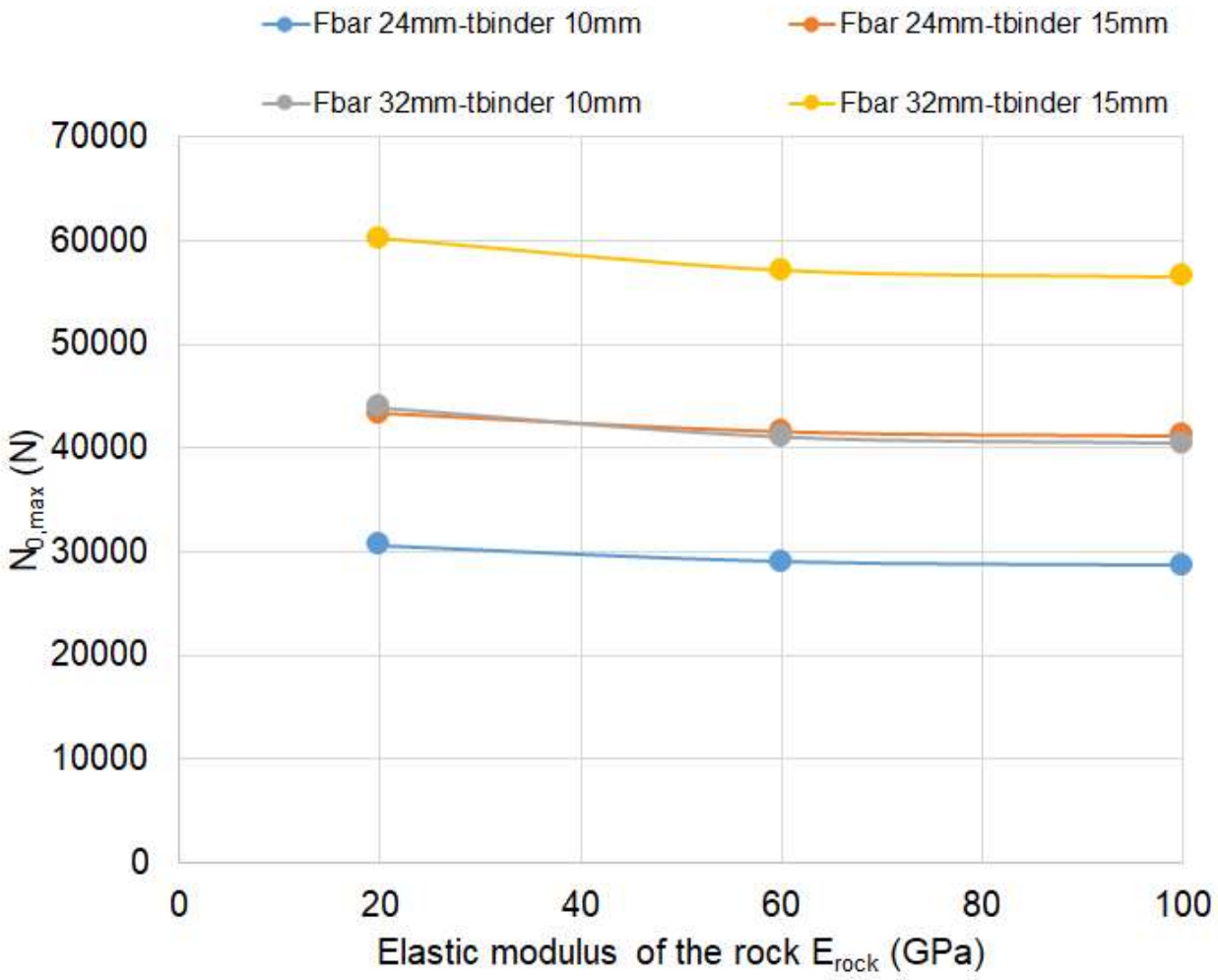

Figure 13. Trend of the axial stabilization force $N_{0,max}$, as the elastic modulus of the rock E_{rock} varies, for different combinations of the thickness of the binder annulus (t_{binder}) and of the angle ϑ which forms the displacement vector of the block δ with the direction of the bolt axis. Case of a resin binder (E_{binder}=2 GPa).

From an examination of the figures, it can be seen that:

- The elastic modulus of the rock E_{rock} does not always have a significant influence on the value of the force $N_{0,max}$
- the angle ϑ, the thickness of the binder annulus, the diameter of the bar and the type of binder used, greatly influence the value of the force $N_{0,max}$

- as the rock's elastic modulus E_{rock} increases, the stabilization force $N_{0,max}$ tends to decrease; this reduction is more evident when traditional cementitious grout is used as binder material
- the angle ϑ has no effect on $N_{0,max}$, whose value, however, is influenced by the diameter of the bar, the thickness of the binder annulus and above all by the type of binder material used (traditional cementitious grout or resin)

The same graphs shown in this paragraph can be used for different values of the diameter of the bar, thickness of the binder annulus, angle ϑ and elastic modulus of the rock: in these cases, linear interpolation can be used to estimate the stabilization forces for values different from those considered in the study, without committing significant errors. If, for example, it is necessary to determine the stabilization force $T_{0,max}$ in the case of a bar diameter Φ_{bar} of 28 mm, thickness of the binder annulus tbinder of 13 mm, angle ϑ of 50° and E_{rock}=50 GPa, adopting the traditional cementitious grout, the following values of $T_{0,max}$ can be obtained from Figures 8 and 9:

$T_{0,max}$ (Φ_{bar}=24 mm; t_{binder}=10 mm; ϑ =45°; E_{rock}=20 GPa) =2759 N

$T_{0,max}$ Φ_{bar}=24 mm; t_{binder}=10 mm; ϑ =45°; E_{rock}=60 GPa) =3452 N

from which we have by interpolation:

$T_{0,max}$ Φ_{bar}=24 mm; t_{binder}=10 mm; ϑ =45°; E_{rock}=50 GPa) =3278 N

$T_{0,max}$ (Φ_{bar}=24 mm; t_{binder}=10 mm; ϑ =60°; E_{rock}=20 GPa) =4778 N

$T_{0,max}$ Φ_{bar}=24 mm; t_{binder}=10 mm; ϑ =60°; E_{rock}=60 GPa) =5978 N

from which we have by interpolation:

499 $T_{0,max}$ (Φ_{bar}=24 mm; t_{binder}=10 mm; ϑ =60°; E_{rock}=50 GPa) =5678 N

500

501 and then again by interpolation:

502 $T_{0,max}$ (Φ_{bar}=24 mm; t_{binder}=10 mm; ϑ =50°; E_{rock}=50 GPa) =4078 N

503

504 Proceeding in the same way for Φ_{bar}=32 mm and t_{binder}=10 mm we have:

505 $T_{0,max}$ (Φ_{bar}=32 mm; t_{binder}=10 mm; ϑ=50°; E_{rock}=50 GPa) =6286 N

506

507 For Φ_{bar}=24 mm and t_{binder}=15 mm we obtain:

508 $T_{0,max}$ (Φ_{bar}=24 mm; t_{binder}=15 mm; ϑ =50°; E_{rock}=50 GPa) =8231 N

509

510 For Φ_{bar}=32 mm and t_{binder}=15 mm we obtain:

511 $T_{0,max}$ (Φ_{bar}=32 mm; t_{binder}=15 mm; ϑ =50°; E_{rock}=50 GPa) =11109 N

512

513 And, therefore, by interpolating the last 4 values of $T_{0,max}$ in pairs, we have:

514 $T_{0,max}$ (Φ_{bar}=28 mm; t_{binder}=10 mm; ϑ=50°; E_{rock}=50 GPa) =5182 N

515 $T_{0,max}$ (Φ_{bar}=28 mm; t_{binder}=15 mm; ϑ=50°; E_{rock}=50 GPa) =9670 N

516

517 And finally:

518 $T_{0,max}$ (Φ_{bar}=28 mm; t_{binder}=13 mm; ϑ=50°; E_{rock}=50 GPa) =7875 N

519

Conclusions

Fully grouted passive bolts take load when the block of rock tends to move, sliding along one or more surfaces formed by the natural discontinuities of the rock. The bolt is able to apply two stabilizing forces to the block: an axial force and a transversal one, perpendicular to the axis of the bolt, with vector belonging to the same plane of the bolt itself and the displacement vector of the rock block. In this paper it was possible to provide simplified equations able to determine the two stabilizing forces of the passive bolt.

- These equations require the determination of the two fundamental mechanical parameters governing the bolt-rock interaction: the shear interaction parameter β_c at the bolt-rock interface and the normal interaction parameter k at the same interface.
- The interaction parameters are difficult to determine through specific in situ tests.
- For this reason, an accurate analysis through numerical modeling is necessary. Two different highly detailed numerical models have been developed, one for the study of the shear interaction and the other for the normal interaction between the bolt and the rock.
- Numerous cases were considered, varying the diameter of the steel bar, the thickness of the binder annulus, the mechanical characteristics of the rock and of the binder material.
- The parametric analysis was developed considering fields of variability of each geometric and mechanical parameter, typical of the real cases that can be encountered.
- From the study it was possible to identify the interaction parameters for all the cases analyzed and also to define equations that are able to estimate them when the main geometric and mechanical parameters that characterize the functioning of fully grouted passive bolts vary.

- Thanks to the knowledge of these parameters, it has been possible to directly evaluate the stabilization forces of the single bolt and develop diagrams that allow their determination as the diameter of the steel bars, the thickness of the binder annulus, the mechanical characteristics of the rock and the binder vary material (either cementitious grout or resin).
- These diagrams are a useful tool to allow an accurate design of such interventions in the stabilization of potentially unstable blocks of rock.

Conflict of interests

Authors declare they have no conflict of interest.

References

Aldrian, W., Wyink, U. & Herrmann, C., 2019. Bolting with pumpable reactive resins-more than fixation of steel dowels in rocks. Geomechanics and Tunnelling, 12(2), 168-174.

Aziz, N., Rasekh, H., Mirzaghorbanali, A., Yang, G., Khaleghparast, S., Nemcik, J. (2018). An Experimental Study on the Shear Performance of Fully Encapsulated Cable Bolts in Single Shear Test. Rock Mechanics and Rock Engineering, 51, 2207–2221

Bajwa, P.S. Hagan, P. and Li, D. (2017) A comparison between resin and a cementitious material in the grouting of cable bolts. In Aziz, N. and Kininmonth, B. (eds.), Proceedings of the 17th Coal Operators' Conference, Mining Engineering, University of Wollongong, 8-10 February 2017, 193-203.

Bawden, F. W., 2011. Ground control using cable and rock bolting. In: P. Darling, ed. SME Mining Engineering Handbook. Littleton: Society for Mining, Metallurgy and Exploration, Inc, pp. 616-617.

567 Carranza-Torres, C., 2009. Analytical and numerical study of the mechanics of rockbolt
568 reinforcement around tunnels in rock masses. Rock Mechanics and Rock Engineering, 42,
569 175–228.

570 Chappell, B., 1989. Rock bolts and shear stiffness in jointed rock mass. Journal of
571 Geotechnical Engineering, 115(2), 179-197.

572 Chen, J., Hagan, P.C., Saydam, S. (2017). Sample diameter effect on bonding capacity of
573 fully grouted cable bolts. Tunnelling and Underground Space Technology 68, 238–243.

574 Craig, P. and Murnane, B. (2013). In-situ pull testing of cable bolts encapsulated with
575 injection polyurethane, 13th Coal Operators' Conference, University of Wollongong, The
576 Australasian Institute of Mining and Metallurgy & Mine Managers Association of Australia,
577 2013, 131-136.

578 DIN 21521-1 (1990). Gebirgsanker für den Bergbau und den Tunnelbau; Begriffe. Beuth
579 Verlag GmbH, Berlin.

580 Indraratna, B. & Kaiser, P. K., 1990. Design for grouted rock bolts based on the convergence
581 control method. International Journal of Rock Mechanics and Mining Sciences &
582 Geomechanics Abstracts, 27(4), 269-281.

583 Gambarova, P.G. 1981. On aggregate interlock mechanism in reinforced concrete plates
584 with extensive cracking. Final report, IABSE colloquium on advanced mechanics of
585 reinforced concrete, vol. 34. International Association for Bridge and Structural Engineering,
586 IABSE, 99–120.

587 Kaiser, P.K., Yazici, S., Nose, J., 1992. Effect of stress change on the bond strength of fully
588 grouted cables. Int. J. Rock Mech. Min. Sci. Geomech. Abstr. 29, 293–305.

589 Kilic, A., Yasar, E., Celik, A.G. (2002). Effect of grout properties on the pull-out load capacity
590 of fully grouted rock bolt. Tunnelling and Underground Space Technology 17, 355–362.

591 Lang, T., 1961. Theory and practice of rock bolting. Transactions of the American Institute
592 of Mining, Metallurgical, and Petroleum Engineers, 220, 333-348.

593 Li C, Stillborg B. 1999. Analytical models for rock bolts. International Journal of Rock
594 Mechanics and Mining Sciences, 36(8):1013e29.

595 Li, Y. et al., 2016. Experimental and numerical investigations on mechanical property and
596 reinforcement effect of bolted jointed rock mass. Construction and Building Materials, 126,
597 843-856.

598 Li, C.C., Kristjansson, G., Håvard Høien, A. (2016). Critical embedment length and bond
599 strength of fully encapsulated rebar rockbolts. Tunnelling and Underground Space
600 Technology 59, 16–23.

601 Li, F., Jin, H., Hu, D., Wang, B. Jia. (2017). Influence of temperature and roughness of
602 surrounding rocks on mechanical behavior of rock bolts. Soil Dynamics and Earthquake
603 Engineering 103, 55–63.

604 Ljungberg, J. (2016). Pullout test of rock bolts at the Lima Hydropower station. MSc Thesis,
605 Royal Institute of Technology, Sweden.

606 Moosavi, M., Bawden, W. F., & Hyett, A. J. (2002) Mechanism of bond failure and load
607 distribution along fully grouted cable-bolts, Mining Technology, 111, 1, 1-12, DOI: 10.1179/

608 Moosavi M, Jafari A, Khosravi A. 2005. Bond of cement grouted reinforcing bars under
609 constant radial pressure. Cement and Concrete Composites, 27(1):103e9.

610 mnt.2002.111.1.1

611 Oreste, P.P. (2009). Face stabilisation of shallow tunnels using fibreglass dowels.
612 Proceedings of the Institution of Civil Engineers: Geotechnical Engineering, 162(2), 95–109.

613 Oreste, P.P. (2009). The dimensioning of dowels for the stabilization of potentially unstable
614 rock blocks on the walls of underground chambers. Geotechnical and Geological
615 Engineering, 27(1), 53–69.

616 Oreste, PP, Cravero, M. (2008). An analysis of the action of dowels on the stabilization of
617 rock blocks on underground excavation walls. Rock Mech Rock Eng; 41(6): 835–868, DOI
618 10.1007/s00603-008-0162-2.

619 Oreste, P. & Dias, D., 2012. Stabilisation of the excavation face in shallow tunnels using
620 fibreglass. Rock Mechanics and Rock Engineering, 45(4), 499-517.

621 Oreste, P. & Spagnoli, G., 2020. A simplified mathematical approach for the evaluation of
622 the stabilizing forces applied by a passive cemented bolt to a sliding rock block. Tunnelling
623 and Underground Space Technology, 103, 103459,
624 https://doi.org/10.1016/j.tust.2020.103459

625 Ranjbarbia M, Fahimifar A, Oreste P. (2014). A simplified model to study the behavior of
626 pre-tensioned fully grouted bolts around tunnels and to analyze the more important
627 influencing parameters. J Min Sci 2014; 50(3): 533-548.

628 Ranjbarnia, M., Fahimifar, A. & Oreste, P., 2016. Practical method for the design of
629 pretensioned fully grouted rockbolts in tunnels. International Journal of Geomechanics,
630 16(1), 04015012.

631 Salcher, M., Bertuzzi, R. (2018). Results of pull tests of rock bolts and cable bolts in Sydney
632 sandstone and shale. Tunnelling and Underground Space Technology 74, 60–70.

633 Spagnoli, G., Carnelli, D., Wyink, U. & Herrmann, C., 2021. Laboratory tests of fully grouted
634 bolts with a pumpable thixotropic resin. In: M. Barla, A. Di Donna & D. Sterpi, eds.
635 Challenges and Innovations in Geomechanics. Cham: Springer, 867–874.

636 Stillborg B. 1994. Professional users handbook for rock bolting. 2nd ed. TransTech
637 Publications.

638 Windsor, C.R., Thompson, A.G., 1993. Rock reinforcement – technology, testing design and
639 evaluation. In: Hudson, J.A. (Ed.), Comprehensive Rock Engineering. Pergamon Press,
640 Oxford.